ARL-TR-9742 ● AUG 2023

Damage Assessment of InGaP-based Power Devices Exposed to Simulated Alpha Radiation

by Nicholas P Barbieri, Marc Litz, John Derek Demaree, Muhammad R Khan, LeighAnn Larkin, Michael Restaino, Michael Wraback, and Vijay Parameshwaran

NOTICES

Disclaimers

The findings in this report are not to be construed as an official Department of the Army position unless so designated by other authorized documents.

Citation of manufacturer's or trade names does not constitute an official endorsement or approval of the use thereof.

Destroy this report when it is no longer needed. Do not return it to the originator.

ARL-TR-9742 ● AUG 2023

Damage Assessment of InGaP-based Power Devices Exposed to Simulated Alpha Radiation

Nicholas P Barbieri and Michael Restaino
General Technical Services, LLC

Marc Litz, John Derek Demaree, LeighAnn Larkin, Michael Wraback, and Vijay Parameshwaran
DEVCOM Army Research Laboratory

Muhammad R Khan
University of Maryland

REPORT DOCUMENTATION PAGE

1. REPORT DATE	2. REPORT TYPE	3. DATES COVERED	
		START DATE	END DATE
August 2023	Technical Report	3/19/21	9/30/23

4. TITLE AND SUBTITLE
Damage Assessment of InGaP-based Power Devices Exposed to Simulated Alpha Radiation

5a. CONTRACT NUMBER	5b. GRANT NUMBER	5c. PROGRAM ELEMENT NUMBER
5d. PROJECT NUMBER	**5e. TASK NUMBER**	**5f. WORK UNIT NUMBER**

6. AUTHOR(S)

Nicholas P Barbieri, Marc Litz, John Derek Demaree, Muhammad R Khan, LeighAnn Larkin, Michael Restaino, Michael Wraback, and Vijay Parameshwaran

7. PERFORMING ORGANIZATION NAME(S) AND ADDRESS(ES)

DEVCOM Army Research Laboratory
ATTN: FCDD-RLA-GA
Adelphi, MD 20783

8. PERFORMING ORGANIZATION REPORT NUMBER
ARL-TR-9742

9. SPONSORING/MONITORING AGENCY NAME(S) AND ADDRESS(ES)	10. SPONSOR/MONITOR'S ACRONYM(S)	11. SPONSOR/MONITOR'S REPORT NUMBER(S)

12. DISTRIBUTION/AVAILABILITY STATEMENT
DISTRIBUTION STATEMENT A. Approved for public release: distribution unlimited.

13. SUPPLEMENTARY NOTES
ORCID IDs: Marc Litz, 0000-0003-0694-4152; John Derek Demaree, 0000-0001-8244-4761

14. ABSTRACT
The effects of radiation damage on an indium gallium phosphide (InGaP) betavoltaic PIN diode and a zinc sulfide/InGaP beta-photovoltaic structure were evaluated by exposing both materials to a beam of 4.5-MeV helium ions as a surrogate for exposure to alpha particles. These measured results will influence the choice of semiconductor and phosphor materials for use in long-lived radioisotope power sources.

15. SUBJECT TERMS
betavoltaic, radioisotope, alpha radiation, radiation damage, semiconductor materials, Energy Sciences

16. SECURITY CLASSIFICATION OF:			17. LIMITATION OF ABSTRACT	18. NUMBER OF PAGES
a. REPORT	b. ABSTRACT	C. THIS PAGE		
UNCLASSIFIED	UNCLASSIFIED	UNCLASSIFIED	UU	41

19a. NAME OF RESPONSIBLE PERSON	19b. PHONE NUMBER *(Include area code)*
Nicholas Barbieri	301-394-4627

STANDARD FORM 298 (REV. 5/2020)
Prescribed by ANSI Std. Z39.18

Contents

List of Figures

List of Tables

1. Introduction

In this work, we measure the radiation tolerance of an indium gallium phosphide (InGaP) photovoltaic (PV) and a zinc sulfide (ZnS) phosphor using a beam of 4.5-MeV helium ions obtained from a Pelletron as a surrogate for alpha particle irradiation. From these measurements, a radiation tolerance parameter for each system is obtained to assess their potential for use in compact, high-energy-density alpha-emitter radioisotope energy sources.

The semiconductor materials are modelled using Stopping and Range of Ions in Matter (SRIM) to compare energy deposition and defect creation to the measured results. Diode structures of these semiconductors are grown, fabricated, and evaluated for use as a direct alphavoltaic (αV) and as an indirect alpha-photovoltaic (αPV) energy converter by monitoring the diode performance continually during ion beam exposure. The radiation-induced degradation of the system was then assessed in terms of power output and its relationship to the fluence of particles incident on the operating diode.

2. Overview

Alpha radiation from ^{241}Am (5.486 MeV) generates electron-hole pairs (EHPs) in a semiconductor device that can be collected to create a continuous trickle charge of current, but alpha particle impacts create dislocations and defects as they deposit energy in semiconductors. Wide bandgap (WBG) semiconductors (silicon carbide [SiC] and gallium nitride [GaN]) and ultrawide bandgap (UWBG) semiconductors (aluminum nitride [AlN] and diamond) are more radiation tolerant than smaller bandgap materials such as Si and InGaP by virtue of their larger, shorter lattice constants and larger displacement energies. Characteristics of these bulk materials, including luminosity and energy conversion efficiency, are evaluated to characterize the effects of radiation damage.

Beta-emitting isotopes have been utilized to create radioisotope power sources generating nanowatts of power per square centimeter.[1–5] The energy density of radioisotopes far exceeds that of any chemical fuel. The decay products of alpha-emitting radioisotopes generate 50–1000 times more energy than beta-emitting isotopes per radioactive decay event. Therefore, given the same activity (decays per second) the potential power density of a power source based on alpha emitters is significantly higher than systems based on beta emitters. It is our goal to increase the power density of radioisotope power sources to that of chemical batteries (~10 mW/cc for Pb-acid batteries). The challenge lies in finding materials that can withstand the alpha flux for long periods of time and to quantify this radiation

tolerance. We will measure and document the energy conversion efficiency and alpha degradation rate of semiconductors, phosphors, and scintillators. The work described in this report provides an initial set of data and results for two commonly used materials: an InGaP PV diode and a ZnS phosphor.

Long-lived ^{241}Am (half-life ~432 years) is readily available and commonly used in smoke detectors as a source of alpha particles. The same radioisotope could be used as a source of energy for use in applications that benefit from persistent operation of critical subcircuits and components, such as in sensors and communication gear, if radiation tolerant energy converters could be designed.

InGaP is a semiconductor material that is commonly used as a PV (e.g., EMCO triple junction cells).[6–8] This semiconductor can also be employed in betavoltaic electric generators to obtain electric power from radioisotopes such as tritium and nickel-63.[9,10] Such devices benefit from a long continuous operating lifetime achieved through radioisotope decay, making them desirable for power applications that require extreme device endurance. The radiation tolerance of semiconductors is related to the bandgap of the materials and inversely proportional to the lattice constant. The characteristics of semiconductor materials of interest are compared in Table 1, and there are plans to explore the other WBG and UWBG semiconductors listed here.

Table 1 Characteristics of semiconductor materials of interest[11–14]

Material	Bandgap energy (eV)	Bandgap type	Lattice constant (A)	Density (g/cc)	Displacement energy (eV)
Si	1.12	Indirect	5.53	2.33	12.9
InGaP	2.17	Direct	5.65	4.47	4
SiC	3.26	Indirect	3.086	3.21	38
GaN	3.39	Direct	3.189	6.15	39
AlGaN	~5.3	Direct	3.17	5.86	15
Diamond	5.45	Indirect	3.589	3.5	35
ZnS	3.7	Direct	5.42	4.09	15

InGaP has been considered for both αV[15,9] and αPV arrangements.[10,16] In a direct αV configuration, literature has reported a 90% degradation of the output power of an InGaP αV device after direct exposure to a fluence of 3×10^{12} particles/cm^2 of 5.5 MeV alpha particles.[9] The first part of this study attempts to confirm these results and measure the rate of PV degradation induced by the exposure of InGaP to ion beams that served as a surrogate for an alpha radiation source.

In an αPV configuration, previous literature reported greater radiation tolerance: a 90% degradation of the combined ZnS-on-InGaP system required an alpha particle fluence of 3×10^{19} particles/cm^2.[9] This higher radiation tolerance is ascribed to the

fact that the alpha particles are primarily absorbed in a layer of phosphorescent ZnS (50 μm) and do not reach the underlying InGaP PV, in which the 525-nm photons emitted from the ZnS are converted into electric current. Calculations from SRIM modelling indicate that if the ZnS layer is thicker than 30 μm, the InGaP can be fully shielded from the alpha radiation. However, the phosphorescent material itself will still be subject to degradation by radiation damage, so the second part of this study also includes exposure of an αPV system (ZnS on InGaP) to energetic ion beams, in which the degradation of the ZnS phosphor can be assessed by observing the reduction of power output with increasing ion fluence.

WBG materials with smaller value lattice constants (LCs) are generally expected to be more radiation hard than those with larger spacing between atoms, since smaller LCs generally indicate stronger bonding between the elemental constituents. The displacement energy is the minimum kinetic energy that must be provided to remove an atom from the lattice and create a defect. Of particular interest for future studies, AlGaN has the smallest LC at 3.17 Å and GaN has the largest documented displacement energy at 39 eV, indicating their potential as radiation-tolerant materials. In addition, diamond has a UWBG (5.45 eV), indicating its potential for high energy conversion efficiency devices, since a semiconductor with large bandgap will generate more power per EHP created.

ZnS powders are often used in detection of nuclear radiation[17,18] because of their efficiency in converting charged particle energy into photons. The phosphor is often doped with silver (Ag), copper (Cu), or aluminum (Al) to inhibit some of the many transitions possible and emphasize a particular photon emission output wavelength. Because of ZnS sensitivity, fast response, and rapid quenching, it is often used as a low count rate radiation detector. When utilized as an energy converter, the energy conversion efficiency and the material degradation rate are the properties of interest. As an example, a reasonable amount of ^{241}Am with regard to cost and safety, 10 mCi, would generate 4×10^8 ions/s, and so after 10 years of operation, the fluence onto the ZnS phosphor could total up to 1.7×10^{17} particles/cm^2, so studies up to these fluence levels will be critical to assess the suitability of these systems for long duration power applications.

In this work we irradiate InGaP and ZnS with He^{++} ions from a 1.7-MV Pelletron tandem positive ion accelerator (National Electrostatics model 5SDH-2) located at Aberdeen Proving Ground, Maryland. A gas RF ion source was used, along with the tandem Pelletron accelerator, to produce 4.5-MeV He^{++} ions, roughly equivalent in energy to the alpha particles emitted from most radionuclide alpha emitters. To evaluate radiation damage in InGaP PN as an αV and thick ZnS (on InGaP PN as an αPV), several experimental samples were exposed to ion beams with varying currents (5 and 60 nA/cm^2) to assess any possible rate effects of the

radiation damage. The fluence was allowed to increase to the point where the device operated at only 10% of original efficiency. Since the rate of ion impingement was several orders of magnitude higher than those expected in an operational αPV system, this enabled us to simulate months or years of radiation damage to these devices in a matter of minutes or hours.

The radiation tolerance of ZnS powder, electrophoretically deposited on InGaP, was quantified as a reduction in luminescence of ZnS. This was inferred from real-time power measurements carried out on the InGaP PV cell during radiation exposure test. To monitor device performance, the open circuit voltage, short-circuit current, and maximum power point (MPP) diode characteristics of the InGaP are tracked throughout the exposure.

ZnS radiation exposure was evaluated by calculating the energy that was deposited into the material. Both ionizing and nonionizing energy losses (IEL and NIEL, respectively) are calculated for InGaP and ZnS. The results are compared to other WBG semiconductor materials.

The work described in this report covers the experimental configuration, the numerical modelling of energy deposition by alpha particles, and the measured current-voltage (IV) values describing energy conversion in InGaP PV devices and electrical power output for InGaP and ZnS phosphor layers. The use of these materials represents a first attempt to understand the radiation hardness of these materials for use in large fluence alpha-stimulated energy conversion applications. The effort will be expanded to include WBG and UWBG materials relevant to energy conversion of radioisotope power source applications, including those with smaller LCs, large displacement energies, and larger bandgaps that would be expected to be more radiation-tolerant. This report describes the modeling, fabrication, ion irradiation experiment, and analysis.

3. Theoretical Analysis and Numerical Modelling

The expected interactions of 4.5-MeV alpha particles in InGaP and ZnS were first examined using SRIM: The Stopping and Range of Ions in Matter, a Monte Carlo code[19] used to simulate the path of energetic charged particles through compounds and layered structures, including the generation of point defects through ballistic nuclear collisions, as well as energy deposition via ionization and phonon generation.

The Pelletron, when first used to simulate an alpha source, was configured for a 1-mm-diameter, 10-nA beam of He^{++} ions, and a rate of particle impingement corresponding to an activity of 1.7Ci ^{241}Am. The particle flux density is

$$I_{rad} = \frac{I}{2eA} = \frac{10\ nA}{2 \cdot 1.602 \cdot 10^{-19}\ C \cdot \pi \cdot (0.5\ mm)^2} \cdot \frac{A}{10^9\ nA} \cdot \left(\frac{10\ mm}{1\ cm}\right)^2 = \frac{1000}{2.52 \cdot 10^{-10}} \frac{1}{s \cdot cm^2} = 3.97 \cdot 10^{12} \frac{1}{s \cdot cm^2} \quad (1)$$

Since this corresponds to a radionuclide activity several orders of magnitude higher than can be safely handled, the ion beam intensity was later lowered to currents ranging from 10 pA to 5 nA to carefully examine the rate of device degradation in time frames ranging from minutes to hours. This still represents a significantly enhanced rate of damage, compared to an actual radionuclide source, but is slow enough to allow close observation of the device performance during the irradiation time.

SRIM was used to numerically calculate expected values in these experiments. The simulation estimates the stopping power of a compound by evaluating the linear combination of the stopping powers of its individual elements. Calculations are further refined using the core and bond approach, which calculates the stopping power in compounds by starting with the superposition of stopping powers from the atomic cores and then adding the stopping power from the bonding electrons. This is to correct for the effect of chemical bonds within the compound on the total stopping power.

When alpha particles interact with atoms, they lose energy to three mechanisms: ionization loss, radiation loss and nonionizing interactions. Charged particles interact continuously and display a well-defined range. They do not penetrate as deeply as uncharged particles. Coulomb interactions during ionization impart energy by exciting the electrons in the material to a higher excited state. If the energy is large enough to overcome the bandgap, the excited electrons transition to the conduction band and can move through the lattice (or plasma). The energy deposited by ionization approximately obeys linear energy transfer (LET) where the energy lost as a function of distance, $\partial E/\partial x$, is proportional to $(z^2 \cdot Z)/v$, where z is the charge of the ion, Z is the atomic number of the atoms in the target material, and v is the velocity of the ion (alpha particle in these simulations). Radiative losses alter the speed (energy loss) and direction of the alpha. The alpha emits bremsstrahlung (braking radiation). The intensity of the bremsstrahlung is proportional to $(z^2 \cdot Z)/m$ where m is the mass of the alpha particle. Because m is large for ions, the bremsstrahlung output is small (compared to electron bremsstrahlung). NIEL is described by displacement of atoms in the lattice by alpha particles. The displacement can leave vacancies, creating defects, move atoms to interstitial sites in the lattice, etch the surface of the target materials, and degrade the optical and electronic properties of target materials.

SRIM simulations of 4.5-MeV alpha particles on both InGaP (density 4.47 g/cc) and ZnS (density 2.5 g/cc) were performed to calculate the energy deposited and interactions expected at various depths into these materials. The penetration depth of 4.5-MeV alpha particles in InGaP PVs was numerically calculated as 16.7 µm with a lateral range of ±0.689 µm as shown in the trajectory plot in Fig. 1.

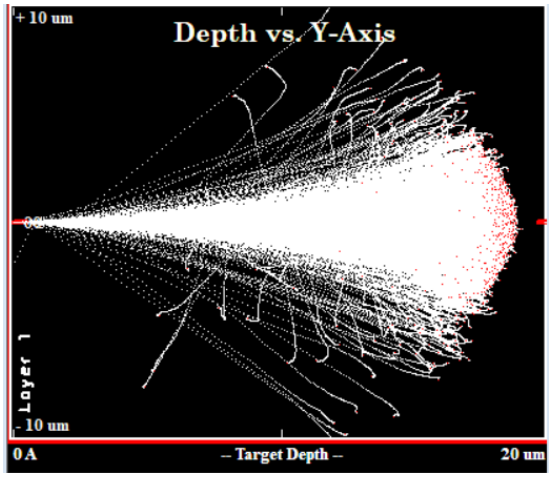

Fig. 1 A SRIM Monte-Carlo calculation of alpha particles' exposure to InGaP shows a longitudinal penetration range of 16.7 µm and lateral range of 1.4 µm diameter

Alpha radiation deposits 200 keV (of the total 4500 keV) in the first 1 µm of InGaP, which is the active region of the InGaP PV, as shown in Fig. 2a. In total, 99.7% of the alpha energy is consumed in ionizing the InGaP, as shown in Fig. 2b. A portion of this energy then goes into the creation of EHPs. Given approximately 6 eV is required to generate an EHP, then each ion can generate at most 33,000 EHPs within the first 1 µm of InGaP. A 10-nA He++ Pelletron current generates 3.125×10^{10} He++ ions/s. Given the 33,000 maximum number of EHPs per ion in the first 1 µm , this can produce at most 1.03×10^{15} EHPs/s corresponding to a maximum 165 µA.

From SRIM calculations, as shown in Fig. 2d, it was determined that the total number of expected collisions per ion (passing through the entire range) is 156 collisions per ion. However, only 1 collision is expected in the first 1 µm active region.

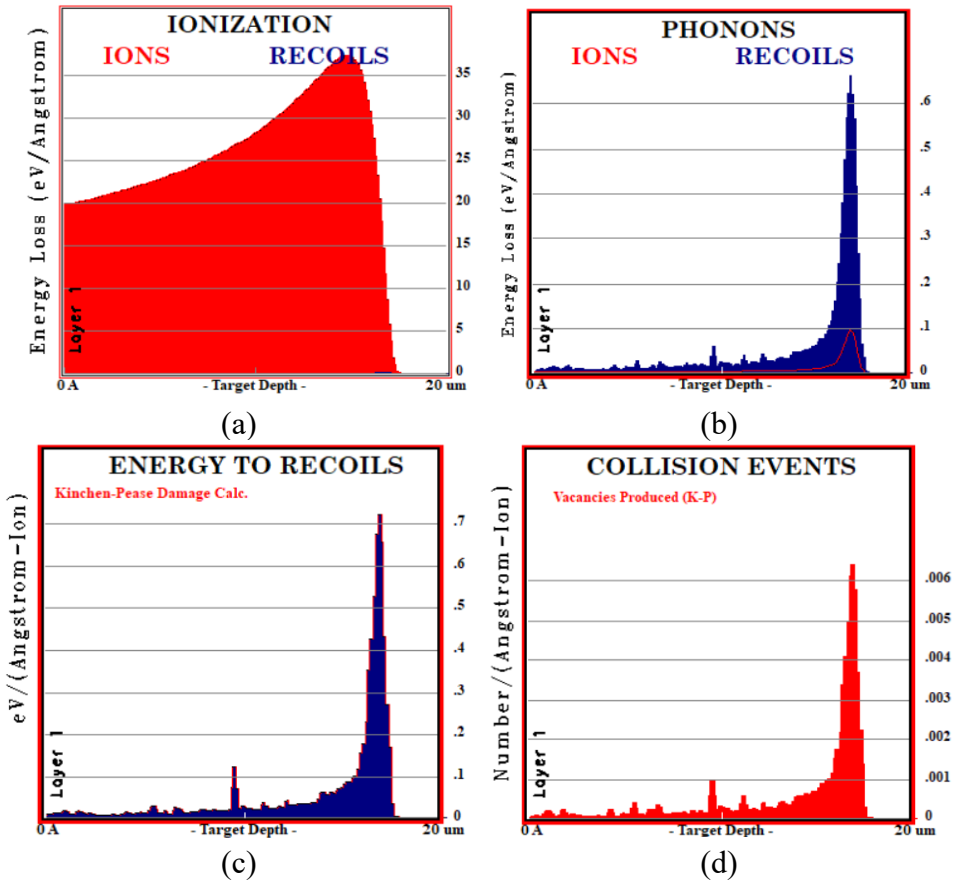

Fig. 2 (a) The IEL in the first 1-µm depth of InGaP is 200 keV/µm. (b) The energy loss to phonons generated by primary alpha in the first 1 µm is ~100 eV/µm. (c) The energy loss to recoils generated by primary alpha in the first 1 µm is <100 eV/µm/ion. (d) The number of collisions within the first 1 µm is <1.

SRIM simulations using 4.5-MeV alpha particles were also executed for ZnS of density 2.5 g/cc. In these simulations, a maximum penetration depth of 26 µm with a lateral range of ±0.904 µm, calculated for 4.5-MeV alpha particles is shown in Fig. 3. The depth at which maximum ionization occurs is 23 µm as shown in Fig. 4a. The depth at which maximum nonionizing loss occurs is 26 µm as shown in Fig. 4d.

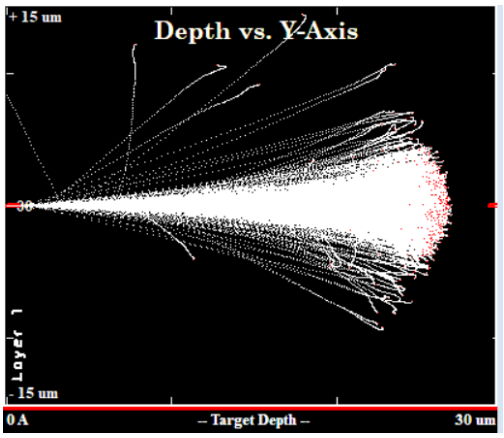

Fig. 3 **A SRIM Monte-Carlo calculation of 4.5-MeV alpha particles' exposure to ZnS shows a longitudinal penetration range of 26 µm and lateral range of 1.8 µm diameter**

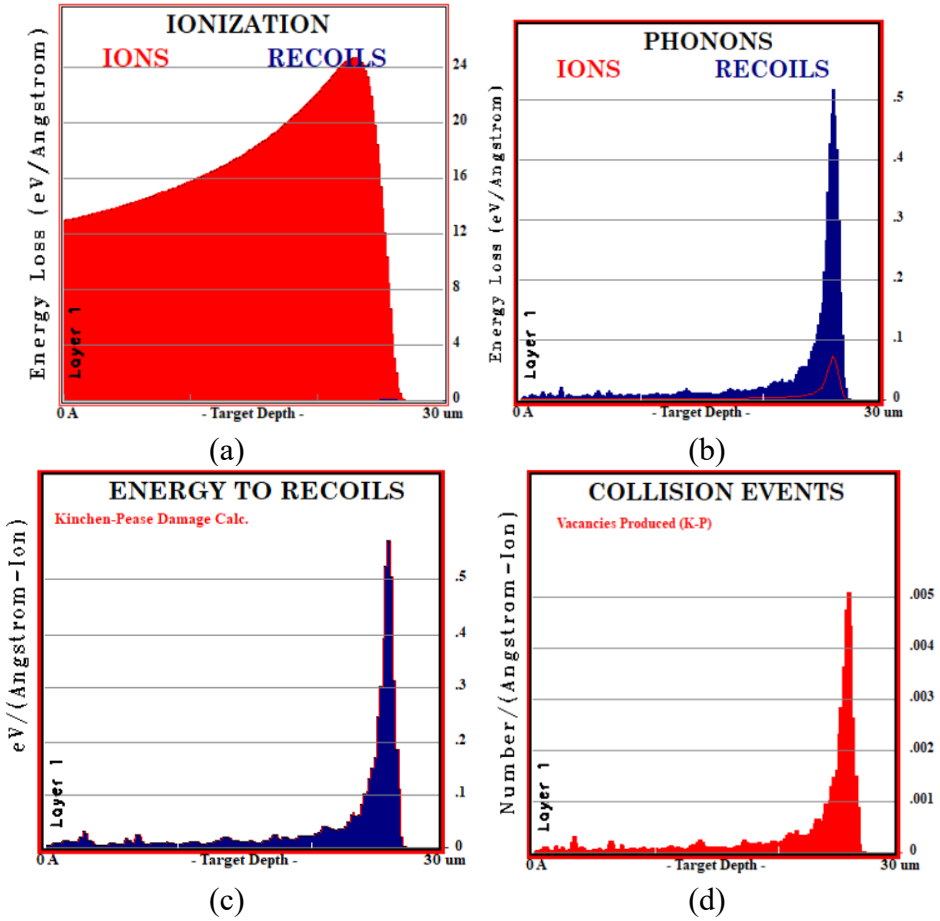

Fig. 4 **(a) The IEL in the ZnS in the first 1 µm is 200 keV. The energy loss to phonons generated by primary alpha in the first 1 µm depth of ZnS is 130 keV. (c) The energy loss to recoils generated by primary alpha in the first 1 µm depth of ZnS is <100 eV. (d) The number of collisions per ion within the first 1 µm is <1.**

Irradiating ZnS with 4.5-MeV (720 nJ/alpha) He^{++} ions resulted in the ionization of ZnS with a 33% efficiency (240 nJ) as shown in Fig. 4a. Initially, more energy was lost per collision event. As alpha particle energy decreased, collisions simultaneously became more frequent but with less energy loss per collision.

The calculated penetration range for 4.5-MeV alpha particles is 17 and 26 μm for InGaP (4.47 g/cc) and ZnS (2.5 g/cc), respectively, as shown in Table 2. The alpha range in InGaP far exceeds the charge collection volume for the semiconductor PN junction needed to extract the generated EHP. Therefore, the InGaP device is not optimized for the conversion of alpha particles to electrical power. The 30-μm range of alpha particles in ZnS is the minimum thickness need to protect the underlying InGaP from radiation damage by reducing the energy of the alpha particles before they reach the PV layer. To fabricate these αPVs, we deposited layers of ZnS of at least 30 μm to protect the underlying InGaP. The penetration range of light in ZnS is approximately 150 μm.[16] Therefore, increasing the thickness by a few extra micrometers of ZnS will not significantly impede fluorescent light from reaching the InGaP for energy conversion and will serve to protect the PV.

Table 2 SRIM tabulated results comparing ZnS and InGaP

Material	Penetration range (μm)	Energy loss (keV)		Displacements (1/ion)
		Ionized	Nonionized	
InGaP	17	4488	12	147
ZnS	26	4485	15	159

4. Sample Preparation

The electrophoretic deposition (EPD) electrolyte is made with isopropyl alcohol (IPA), nitrate salt of 63 mg $Mg(NO_3)^2 \cdot 6H_2O$, and 3000 mg of a ZnS phosphor doped with Cu and Al. The salt was added to 269 g of IPA solution, and the solution was sonicated for 180 s to dissolve the salt, and then again for 380 s after 1.5 g of phosphor was added into it. The mixture was mechanically stirred right before the EPD started.

The EPD was carried out by placing the InGaP and the counter electrode in a wafer carriage at a separation distance of about 8 mm. The carriage is then dipped into the solution, and an applied voltage of 100 V is applied to the electrodes for 50 min. After the first 25 min, the solution was stirred mechanically, and the EPD continued for another 25 min. The InGaP samples were then air-dried before the ZnS deposition thickness was measured using a stylus profilometer.

Two samples were fabricated for the alpha exposure. The first is a 1-cm^2 InGaP PV cell (#G4) mounted on copper plate. The second sample had an 81-µm-thick layer of ZnS electrophoretically deposited on the InGaP PV (#F12). The ZnS deposited sample shown in Fig. 5 has an 81-µm-thick layer over a 9 × 9 mm^2 area. The mass of the ZnS deposition is 0.015 g, resulting in a ZnS density of 2.29 g/cc.

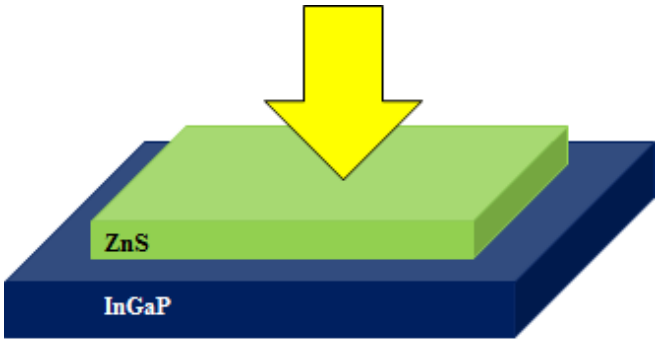

Fig. 5 A 10-nA alpha beam irradiates an 81-µm-thick layer of ZnS (9 × 9 mm^2) deposited on 1 cm^2 InGaP as measured by light output. ZnS volume 6.56 mm^3 and density 2.29 g/cc.

5. Experimental Setup

Two devices were evaluated. The first device is a pure InGaP PIN diode to be used as an αV. The second device is an InGaP PIN diode coated with an 81-µm layer of ZnS to be used as an αPV. The intent of this selection is to compare the performance of an αV device to that of an αPV device. The investigation is focused on identifying the alpha fluence required to reduce PIN current output to 25% of its original value.

Both devices were exposed to beams of 4.5-MeV helium ions that served as a surrogate for the alpha radiation typical of radionuclide sources. For each device, separate spots on the device surface were exposed at different rates to determine if radiation degradation was purely a function of incident fluence, or if it was also dependent upon the flux density of the alpha particles. Should the former case be proven true, this will enable future experiments to substitute short-duration, high-exposure-rate tests for long-duration, low-exposure-rate tests, enabling the rapid evaluation of radiation for low-power, long-duration αV devices.

Prior to alpha radiation exposure, IV curve measurements were taken of both devices using a Keithley 2450 source meter. The source meter was controlled by a Raspberry Pi microcontroller and continuously acquired and recorded IV curves throughout the radiation exposure experiment,[20] both prior to and during radiation

exposure. Measurements taken prior to radiation exposure were used to establish baseline performance before radiation damage occurs.

Beams of 4.5-MeV He^{++} ions were produced using a National Electrostatics 5SDH-2 positive ion accelerator operating at 1.5 MV. The accelerator is a tandem style accelerator in which negative He^{-} ions are extracted from an RF gas plasma and accelerated toward the high-voltage terminal, where electrons are stripped off the approximately 1.5 MeV ions by a region of relatively higher-pressure nitrogen gas. He^{++} ions created in the terminal stripper region are then accelerated away from the terminal, gaining another 3 MeV of energy, for a final energy at the end station of 4.5 MeV. The devices to be tested were placed within a vacuum chamber located at the end of the Pelletron beam line, shown in Fig. 6, and a combination of magnetic and electrostatic lenses were used to focus the ion beam to an area approximately 1 mm in diameter on the surface of the devices.

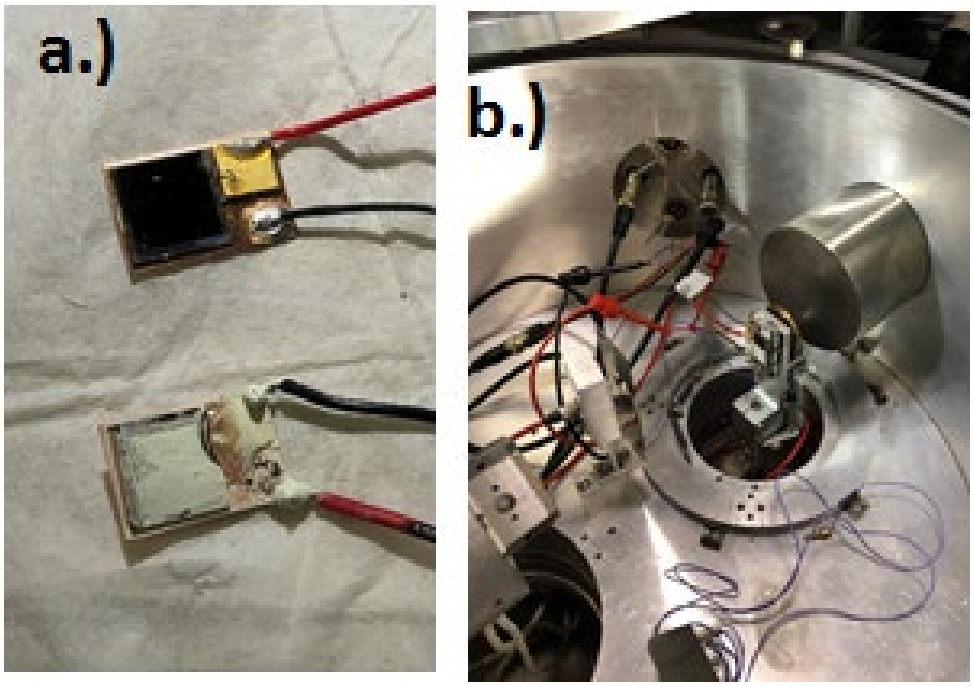

Fig. 6 (a) InGaP PV samples #G4 and ZnS deposited InGaP #F12 before exposure to alpha radiation beam. (b) Samples mounted in vacuum chamber. Beam port is on left.

Each exposure was run for approximately 60 min. During radiation exposure, the source meter was used to continually collect IV measurements, which form the basis of evaluating device degradation resulting from alpha radiation exposure. The IV curves were then used to calculate the MPP, the open circuit voltage (V_{oc}), and the short circuit current (I_{sc}) at each moment during the irradiation.

6. Results

The results described in this section show a comparison of an αV versus an αPV based on two experimental alpha exposures for each of these systems (αV and αPV).

6.1 Alphavoltaic (Pure InGaP)

Two exposure tests were conducted on an InGaP αV wafer. For each test, InGaP was exposed to varying fluxes of 4.5-MeV alpha particles. A summary of the testing parameters is shown in Table 3.

Table 3 InGaP exposure test properties

Test run	Current (pA)	Exposure rate (ion/s)	Radiation power (μW)	Exposure time (min)
221212	160	5.0×10^8	360	65
221221	1800	5.6×10^9	4050	35

The first exposure was conducted using 160 pA of current over a duration of 65 min. The IV measurement for this exposure is shown in Fig. 7. The degradation of the InGaP is observable in the IV curves that slowly reduce in open circuit voltage, V_{oc}, and short circuit current, I_{sc}. These IV curves were used to calculate several circuit parameters associated with the PIN diode, which are shown in Fig. 8.

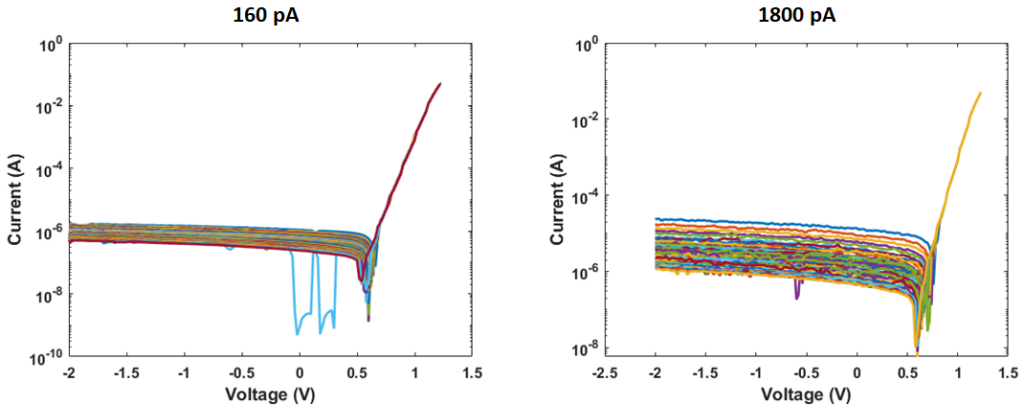

Fig. 7 IV curve measurements taken for the 70-min, 160-pA exposure of InGaP

Device performance during 160 pA exposure is shown in Fig. 8. Device power output slowly degrades over the 65 min of alpha exposure, falling to less than 25% of its original power output by the end of the exposure.

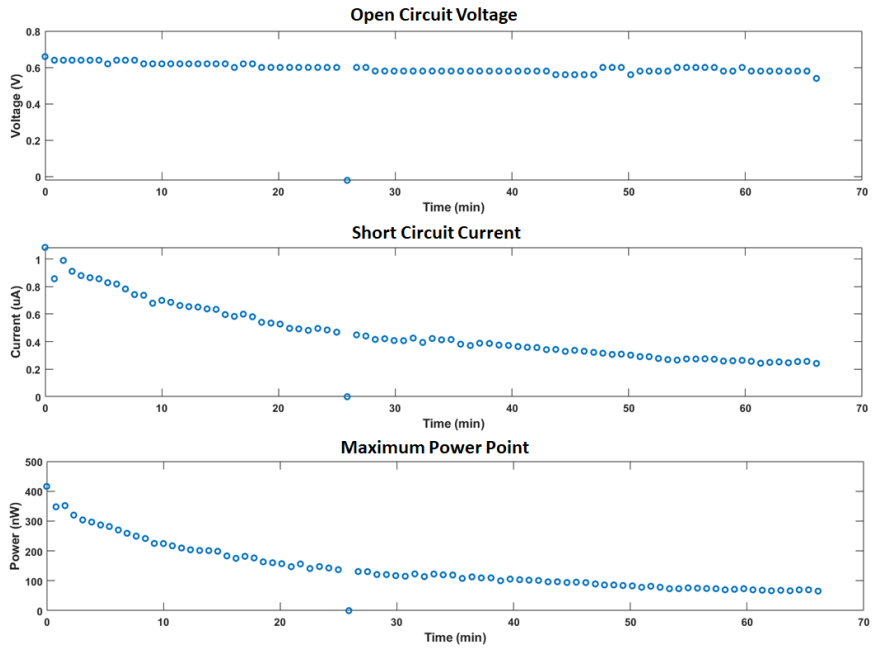

Fig. 8 InGaP betavoltaic property degradation during 160-pA alpha particle exposure. The V_{oc} output is stable at approximately 0.8 V. The current and power is reduced.

The second exposure was conducted with 1800 pA of current over 35 min. The resulting IV curves are shown in Fig. 9. The V_{oc} for the 1800-pA current exposure starts at 0.75 V, which is larger than the V_{oc} for the 160-pA exposure that begins with a V_{oc} of 0.65 V.

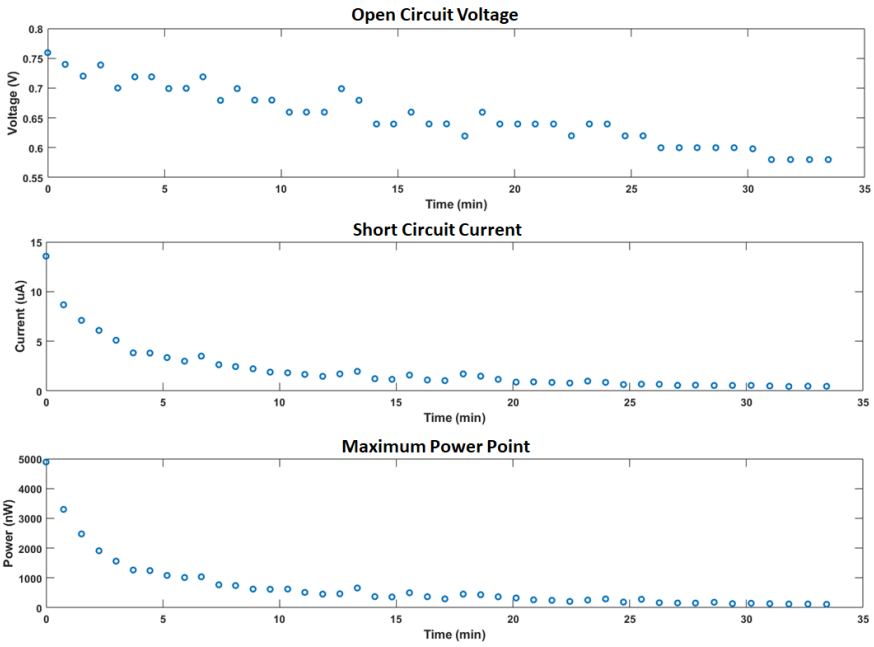

Fig. 9 InGaP betavoltaic property degradation during 1800-pA alpha particle exposure

For the second test, the alpha current and corresponding irradiance of the device was increased by an order of magnitude. The result of this enhanced exposure rate is shown in Fig. 9. For these results, complete device failure is observed within 30 min.

To compare InGaP performance across different flux alpha exposure, exposure time was converted to cumulative particle fluence. Measured device power was then converted to efficiency by dividing through by incident ion power. By parameterizing device performance in terms of fluence, rather than exposure time, different exposure tests can be compared directly. The results are shown in Fig. 10.

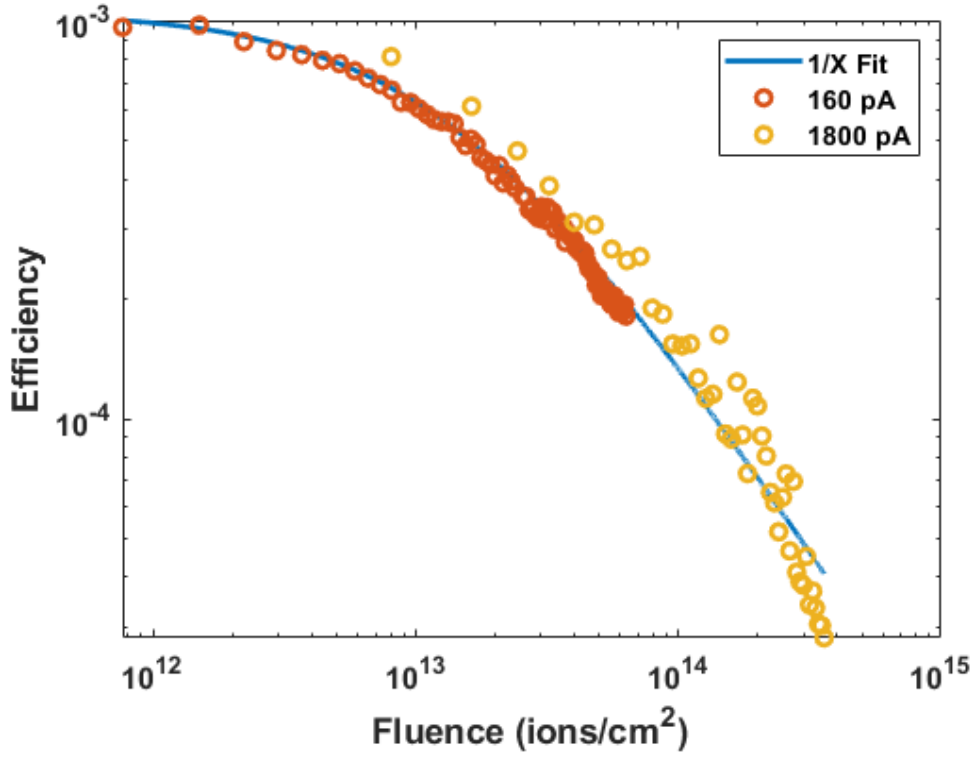

Fig. 10 InGaP efficiency as a function of total ion fluence

A simple model was devised to describe the degradation of device efficiency with fluence. This model is of the functional form:

$$f(\phi) = \epsilon \frac{\phi_0}{\phi+\phi_0} = \frac{\epsilon}{1+\phi/\phi_0} \quad (2)$$

The initial device efficiency, ϵ, and the radiation resistance value, ϕ_0 are the parameters for the fit. The value for ϕ_0 represents the fluence at which the operational capability of the device is reduced to 50% of the initial efficiency. The coefficient ϵ represents the device conversion efficiency prior to radiation damage. This is the function $1/\phi$, but with the singularity found at $\phi = 0$ shifted to

$\phi = -\phi_0$ and the y-intercept set to ϵ. For the InGaP tests shown in Fig. 10, the functional fit was obtained using

$$f(\phi) = 1.1 \cdot 10^{-3} \frac{14\times10^{12}}{\phi+14\times10^{12}} = \frac{1.1\cdot10^{-3}}{1+\phi/14\times10^{12}} \tag{3}$$

From Fig. 10 and excellent correspondence between both exposure tests and the model can be observed.

To evaluate the fitting error on a point-by-point basis, the sum of squares error was divided by the total number of sample points. The root of the resulting quotient was then taken. The resulting fitting error is then expressed as

$$E_f = \sqrt{\frac{1}{N}\sum_n [y_n - f(\phi_n)]^2} \tag{4}$$

where E_f is the fitting error, y_n is the nth device efficiency measurement, $f(\phi)$ is the fitting function, and ϕ_n is the total fluence the device has been exposed to when the nth measurement was taken. Using Eq. 4, a fitting error 9.2×10^{-5} was obtained for InGaP. The MATLAB code use to carry out this analysis is listed in the Appendix.

Standard power degradation laws from literature have the form[6,21]

$$\frac{P_{max}(\phi)}{P_{max}(0)} = a - b\log\left(1 + \frac{\phi}{\phi_0}\right) \tag{5}$$

However, such laws suffer from a significantly inferior fit when compared to the fit obtained using Eq. 2. The error, as evaluated by the sum of squares for Eq. 5 for the 1800 pA data is 1.7×10^{-4}, while that obtained for Eq. 2 is 9.2×10^{-5}; thus, the fit from Eq. 5 has twice the error of a simple $1/X$ fit.

6.2 Alpha-Photovoltaic (ZnS Deposited on InGaP)

A second series of measurements were taken using ZnS-coated InGaP wafers, again using 4.5-MeV alpha particles. The test parameters are summarized in Table 4.

Table 4 ZnS/InGaP exposure test properties

Test run	Current (pA)	Flux (ion/s)	Radiation power (uW)	Exposure time (min)
221209	9	2.8×10^7	20	65
221212	160	5.0×10^8	360	70

Two exposure tests were run at 9 pA for 65 min and 160 pA for 70 min. The resulting IV curves are shown in Fig. 11.

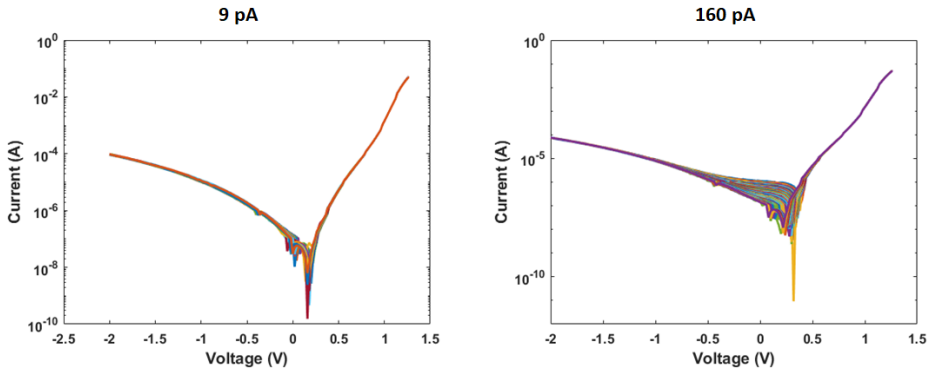

Fig. 11 IV curve measurements acquired for ZnS-coated InGaP shows the reduction in V_{oc} and I_{sc}

The device parameters derived from the IV curves are shown for the 9- and 160-pA exposure tests in Figs. 12 and 13, respectively.

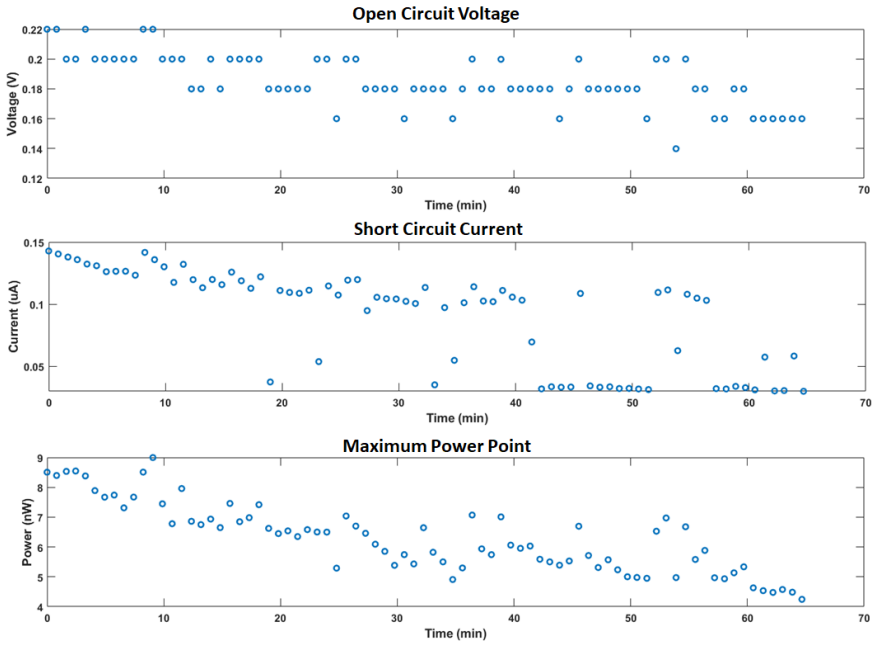

Fig. 12 ZnS/InGaP betavoltaic property degradation during 9-pA exposure test

Device performance during 9 pA of exposure is shown in Fig. 13. These measurements suffered from significant variation in output power due to fluctuating Pelletron ion current, and little device degradation could be observed over the resulting noise.

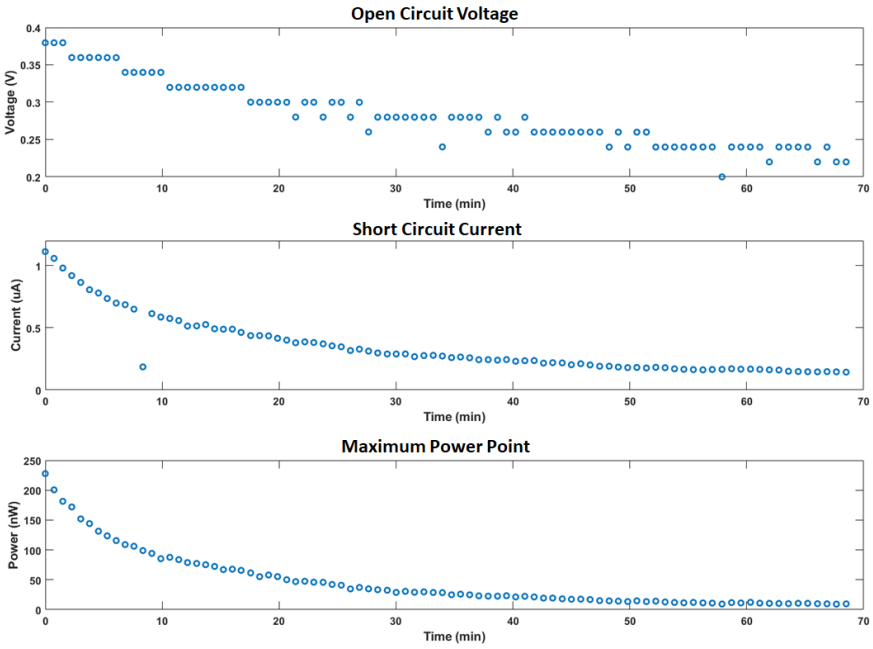

Fig. 13 ZnS/InGaP betavoltaic property degradation during 160-pA exposure test

Device performance during 160-pA exposure is shown in Fig. 14. For this test, device power output undergoes consistent decay throughout the test. Device power output falls below 10% of its initial value at the end of the 70-min exposure.

Both experimental results were converted into measurements of device efficiency as a function of alpha fluence to facilitate comparison. The results of these measurements and the corresponding model are show in Fig. 14.

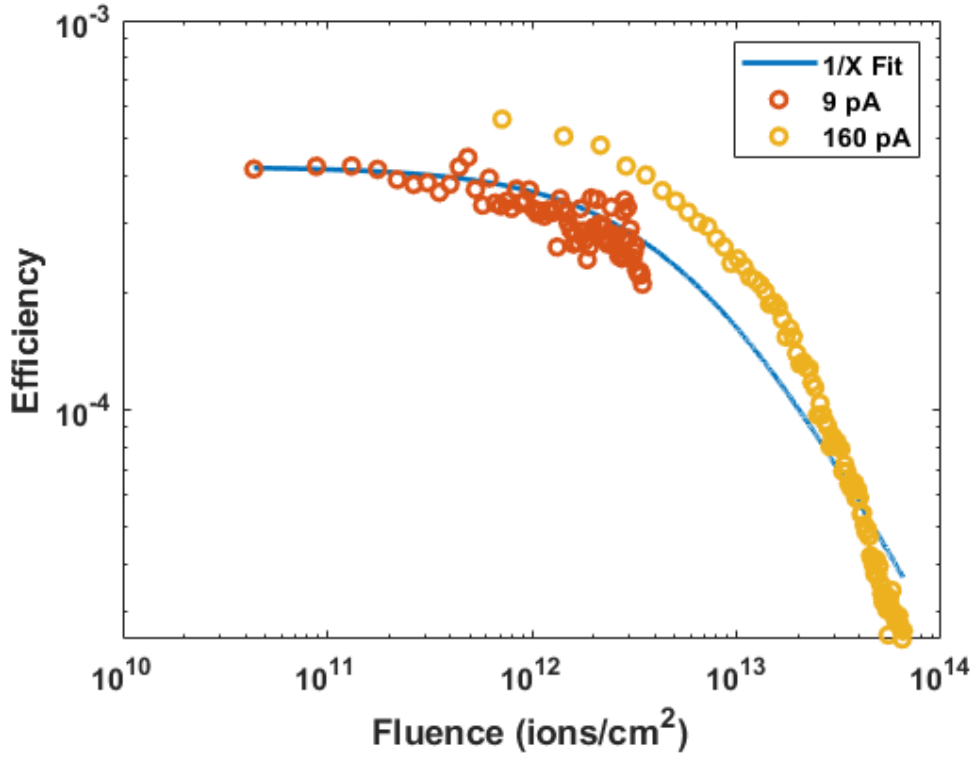

Fig. 14 ZnS/InGaP efficiency as a function of ion fluence

The degradation of ZnS-coated InGaP is described by the same functional form as bare InGaP. As ZnS is a different material, it contains different parameters for the device efficiency and radiation resistance. The function

$$f(\phi) = 4.2 \cdot 10^{-4} \frac{6.3\times10^{12}}{\phi+6.3\times10^{12}} = \frac{4.2\times10^{-4}}{1+\phi/6.3\times10^{12}} \quad (6)$$

was used to fit the ZnS/InGaP data. This fit resulted in a fit error of 8.6×10^{-5}.

The performance of both devices is summarized in Table 5 and illustrated in Fig. 15. Each device can be characterized by its initial efficiency, ϵ, and radiation resistance, ϕ_0, which is the fluence at which the efficiency drops to 50% of the original value. From Table 5 it is clear that bare InGaP provides superior performance to that of ZnS-coated InGaP, possessing triple the initial efficiency and twice the radiation resistance. The energy conversion efficiency for InGaP and ZnS/InGaP calculated from the data is 0.11% and 0.06%, respectively. In comparison, ZnS/InGaP possesses an electron to photon conversion efficiency of 25% for approximately 10 keV electrons.[14] This ratio of alpha to electron energy conversion efficiency is a factor of 500.

Table 5 Radiation analysis results for InGaP and ZnS

Parameter	Variable name	InGaP	ZnS/InGaP
Initial efficiency (ratio)	ϵ	1.1×10^{-3}	4.2×10^{-4}
Radiation resistance (Fluence)	ϕ_0	14×10^{12}	6.3×10^{12}
Fit error (One data set only)	. . .	9.2×10^{-5}	8.6×10^{-5}

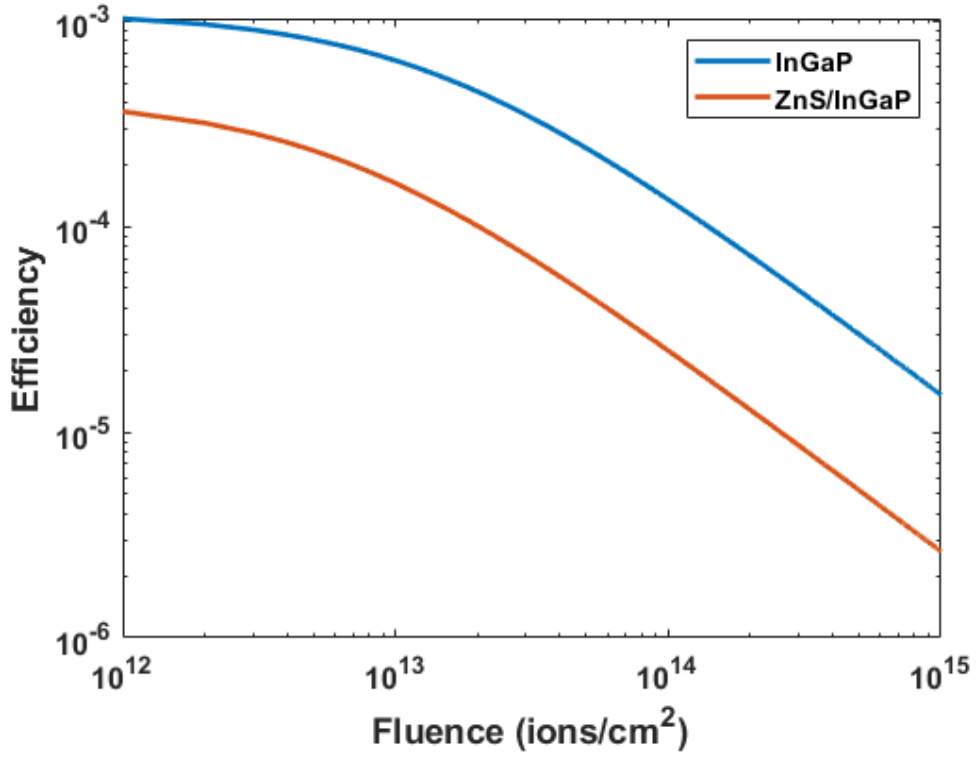

Fig. 15 Efficiency as a function of cumulative fluence as described by Eq. 2 for both InGaP and ZnS/InGaP

7. Conclusions

When exposed to a beam of 4.5-MeV helium ions (surrogates for alpha particles) of variable flux (9, 160, and 1800 pA) over a period of 30 to 70 min, the device performance of several InGaP PIN αV devices could be observed to degrade over time. Device performance degradation could be mapped directly to total particle fluence independent of exposure rate. Such behavior permits short-duration, high-exposure-rate experiments of αV devices to be used as proxies for long-duration, low-exposure-rate experiments. Given that αV devices are intended to operate for years in the field, this provides a valuable tool for rapidly assessing the long-term performance of such devices.

Measured device efficiency degradation to irradiation conforms to an empirically determined $1/x$ fluence power law. When fit to our data, this empirical relation is twice as accurate than the exponential radiation degradation relations often found in literature. The underlying physics of this empirical relation has yet to be determined and should be explored in a future investigation. This power law also enables the performance of αV devices to be summarized using a pair of fit parameters, both of which have clear physical meaning. The first parameter provides the device's conversion efficiency prior to suffering any radiation damage. The second parameter quantifies how resistant a given device is to radiation damage. This should enable rapid and straightforward comparison of the performance of different αV devices.

During the course of these experiments, two separate devices were evaluated: an αV InGaP device and a beta-photovoltaic ZnS/InGaP. Both devices could be quantified using the fit parameters for the $1/x$ fluence power law, and then could be directly compared using those same fit parameters. Using this methodology, it was concluded the InGaP αV diode provided superior performance, as it possessed both superior conversion efficiency and radiation tolerance.

This same methodology should be applied to a wider range of αV devices in the future, both to collect data that would provide a convenient summary of αV device performance and to ensure that the empirical fluence power law is generally applicable. Some modifications to the empirical established radiation degradation law may be required to accommodate future data.

8. References

1. Oh K, Prelas MA, Lukosi ED, Rothenberger JB, J SR, Weaver CL, Montenegro DE, Wisniewski DA. Theoretical maximum efficiency for a linearly graded alphavoltaic nuclear battery. Nucl Technol. 2012;179:2;243–249.
2. Prelas MA, Weaver CL, Watermanm ML, Lukosi ED, Schott RJ, Wisniewski DA. A review of nuclear batteries. Prog Nucl Energy. 2014;75:117–148.
3. Spencer MG, Alam T. High power direct energy conversion by nuclear batteries. Appl Phys Rev. 2019;6:031305.
4. Terranova M. Nuclear batteries. Int J Energy Res. 2022:1–26.
5. Iwan A, Pellowski W, Bogdanowicz A. Conversion of radiophotoluminescence irradiation into electricity in photovoltaic cells. A review of theoretical considerations and practical solutions. Energies. 2021;14:6186.
6. Campesato R, Baur C, Casale M, Gervasi M, Gombia E, Greco E, Kingma A, Rancoita PG, Rozza D, Tacconi M. Effects of irradiation on triple and single junction InGaP/GaAs/Ge solar cells. 35th European PV Solar Energy Conference; 2018 Sep 24–28; Brussels, Belgium.
7. Li J, Aierken A, Liu Y, Zhuang Y, Yang X, Mo J H, Fan RK, Chen QY, Zhang SY, Huang YM, Zhang Q. A brief review of high efficiency III-V solar cells for space application. Frontiers in Physics. 2021;8:631925.
8. Shaps PR, Aiken DJ, Stan MA, Thang CH, Fatemi N. Proton and electron radiation data and analysis of GaInP2/GaAs/Ge solar cells. Prog Photovoltaics Res Appl. 2002;10(6):383–90.
9. Cress CD, Landi BJ, Raffaelle RP, Wilt DM. InGaP alpha voltaic batteries: synthesis, modeling, and radiation tolerance. J Appl Phys. 2006;100(11):114519.
10. Russo J, Ray W 2nd, Litz MS. Low light illumination study on commercially available homojunction photovoltaic cells. Appl Energy. 2017;191:10–21.
11. Yen WM. Phosphor handbook. CRC Press; 2006.
12. Comprehensive reference on semiconductor manufacturing. Lattice constants. EEsemi.com; c2004 [accessed 2023 June 15]. https://eesemi.com/lattice_constants.htm.

13. List of semiconductor materials. Wikipedia; last updated 2023 May 27 [accessed 2023 June 15]. https://en.wikipedia.org/wiki/List_of_semiconductor_materials.

14. Tomm JW, Kernke R, Mura G, Vanzi M, Hempel M, Acklin B. Catastrophic optical damage of GaN-based diode lasers: sequence of events, damage pattern, and comparison with GaAs-based devices. J Electron Mater. 2018;47:4959–4963.

15. Bailey SG, Wilt DM, Castro SL, Cress CD, Raffaelle RP. Photovoltaic development for alpha voltaic batteries. 31st IEEE Photovoltaic Specialist Conference; 2005.

16. Russo J, Litz M, Ray W 2nd, Smith B, Moyers R. A radioluminescent nuclear battery using volumetric configuration: 63 Ni solution/ZnS:Cu, Al/InGaP. Appl Radiat Isot. 2017;130:66–74.

17. D'Amico P, Calzolari A, Ruini A, Catellani A. New energy with ZnS: novel applications for a stand transparent compound. Sci Rep. 2017;7:16805.

18. Yamamoto S, Tomita H. Comparison of light outputs, decay times, and imaging performance of a ZnS(Ag) scintillator for alpha particles, beta particles, and gamma photons. Appl Radiat Isot. 2021;168:109527.

19. Ziegler JF, Ziegler MD, Biersack JP. SRIM – The stopping and range of ions in matter (2010). Nuclear Instrument Methods Physics Research Section B Beams Interactions with Materials and Atoms. 2010;268:181.

20. Barbieri NP. Automated analysis of betavoltaic diode electrical response in damaging radiation environments [master's thesis]. North Carolina State University; 2021.

21. Yamaguchi M, Khan A, Taylor SJ, Imaizumi M, Hisamatsu T, Matsuda S. A detailed model to improve the radiation-resistance of Si space solar cells. IEEE Trans Electron Devices. 1999;46(10):2133–2138.

Appendix. MATLAB Code

The following MATLAB code starts with input, the maximum power point calculated from each current-voltage (IV) curve acquired during the experimental series. Inserting the data series into the code (G4_Data.m) will result in calculation of device efficiency as a function of ion fluence.

```
function [] = Automated_Fit()

%read the data
[F1, Pp1, label1] = G4_Data_2();
[F2, Pp2, label2] = G4_Data_3();

%[F1, Pp1, label1] = G4_Data_2();
%[F2, Pp2, label2] = G4_Data_3();

F = Construct_Fluence_Axis_2(F1, F2);

%compile the datasets
Fc = [F1; F2];
Ppc = [Pp1; Pp2];

%set the startpoint
a = max(Ppc);
b = 3;
start = [a b];
lower = [0 0];
upper = [1 10];

%set n
n = 2.0;

%Specify the fit function
invrat2 = ['a*b^' num2str(n) '/(x + b)^' num2str(n)];

%Perform the automatic fit
[FO, G] = fit(F2, Pp2, invrat2, 'Start', start);
N = max(size(F2));
G.sse*10^8
(G.sse/N)^0.5*(10^4)
G.sse/(FO.a)^2

%construct theoretical fit
Ef = Construct_Rational(F, 2, FO.b, FO.a);

%switch back to number of ions
F1 = F1*10^12;
F2 = F2*10^12;
F = F*10^12;

%prepare the plots
close all;

figure;
```

```
loglog(F1, Pp1, 'o', F2, Pp2, 'o', F, Ef, "Linewidth", 2);
set(gca, 'FontSize', 12, 'FontWeight', 'bold');
xlabel('Fluence (ions)', 'FontSize', 14, 'FontWeight', 'bold');
ylabel('Efficiency', 'FontSize', 14, 'FontWeight', 'bold');
legend(label1, label2, '1/X^2 Fit');
function [F] = Construct_Fluence_Axis_2(F1, F2)

%set the resolution
res = 1000;

%obtain the maximum flux value
Fm = max([max(F1), max(F2)]);

%calculate the increment
inc = Fm/res;

%construct the fluence axis
F = 0:inc:Fm;
F = transpose(F);



function [F] = Construct_Rational(T, n, t0, A)
%construct a nth power inversion rational function
%T is the time axis in minutes
%t0 is the value of x at t = 0 in minutes
%A is the value at t = 0

%construct the rational function
F = 1 - (T/t0).^n;

%take the reciprocal and write the output
F = A*F;
```

```
function [F, Pe, label] = G4_Data_2()

%ion flux
ionf = 1.00*10^9;
%ion/s

%ion power
pion = 0.72;
%ion power in mW

%set the label
label = '160 pA';

%convert to Gion
ionf = 60*ionf*10^-12;

T = [ 0
   0.800000000000000
   1.566666666666667
   2.316666666666667
   3.083333333333333
   3.850000000000000
   4.616666666666666
   5.366666666666666
   6.133333333333334
   6.883333333333334
   7.666666666666667
   8.449999999999999
   9.216666666666667
  10.000000000000000
  10.766666666666667
  11.550000000000001
  12.316666666666666
  13.100000000000000
  13.883333333333333
  14.650000000000000
  15.433333333333334
  16.216666666666665
  16.983333333333334
  17.766666666666666
  18.550000000000001
  19.350000000000001
  20.133333333333333
  20.949999999999999
  21.733333333333334
  22.550000000000001
  23.366666666666667
  24.166666666666668
  24.983333333333334
  25.883333333333333
  26.683333333333334
  27.483333333333334
  28.283333333333335
  29.100000000000001
  29.899999999999999
```

```
  30.716666666666665
  31.533333333333335
  32.350000000000001
  33.166666666666664
  33.966666666666669
  34.783333333333331
  35.600000000000001
  36.433333333333330
  37.233333333333334
  38.066666666666670
  38.883333333333333
  39.700000000000003
  40.516666666666666
  41.316666666666670
  42.133333333333333
  42.950000000000003
  43.750000000000000
  44.566666666666670
  45.366666666666667
  46.183333333333330
  47.000000000000000
  47.783333333333331
  48.583333333333336
  49.366666666666667
  50.166666666666664
  50.966666666666669
  51.750000000000000
  52.549999999999997
  53.350000000000001
  54.149999999999999
  54.950000000000003
  55.750000000000000
  56.533333333333331
  57.333333333333336
  58.116666666666667
  58.916666666666664
  59.716666666666669
  60.500000000000000
  61.299999999999997
  62.083333333333336
  62.883333333333333
  63.683333333333330
  64.466666666666669
  65.266666666666666
  66.083333333333329];
%Time in minutes

%shift the time
T = T + 0.7 + 2/30;

Pp = [0.415969488252320
   0.347680147679800
   0.351757173563250
   0.319803181922140
   0.303811146877550
```

```
0.296467651342800
0.286851518192780
0.281642701948300
0.270034612360560
0.259023607987150
0.249424735323960
0.241464807776840
0.225086185109120
0.224642951663400
0.217045909519200
0.209763710392770
0.203750771439840
0.201406499627550
0.201000194248880
0.198787445703000
0.183229305974000
0.175226743167720
0.181902045605100
0.176477409221290
0.163409786991000
0.160487332563580
0.157082918727240
0.147216740343570
0.156225157020870
0.141081386925540
0.147580798149000
0.142714325969670
0.137197148983300
                0
0.130993715726700
0.130621575589100
0.120964303148700
0.120788897511590
0.117211094612800
0.115152207901560
0.122937533562540
0.114000375825330
0.122612953553100
0.119985796186060
0.119314289786990
0.108032211139120
0.113105613575550
0.109702577114390
0.109739198450840
0.100084461454880
0.105788589084060
0.103615165639680
0.102142028942730
0.101057609022500
0.096503291528800
0.096733397332180
0.094222507574520
0.095280972598350
0.093952552234890
0.089409199010400
```

```
   0.086051550459480
   0.085954761294210
   0.084140891502240
   0.082839787020000
   0.078174689664960
   0.081600077191320
   0.078277474060800
   0.073496765580840
   0.073575393065490
   0.076242481925580
   0.075070364898480
   0.074141995525500
   0.073521584535770
   0.069789739366760
   0.071500993247160
   0.073448828751060
   0.069728072623440
   0.068506028476810
   0.066698038520750
   0.068032893188850
   0.066545364189150
   0.069647964873180
   0.069723582246010
   0.065338751423040];
%Peak power in uW

%convert to fluence
F = T*ionf;

%evaluate the efficiency
Pe = Pp/pion/1000;
```

Bibliography

Other references relevant to this area of investigation are included here. These references were helpful in understanding the topical area and helped refine and design the experimental plan executed in this report.

1. Pearton SJ, Ren F, Patrick E, Law ME, Polyakov AY. Review - ionizing radiation damage effects on GaN devices. ECS J Solid State Sci Technol. 2016;5(2):Q35–Q60.
2. Xue S, Tan C, Kandlakunta P, Oksuz I, Hlinka V, Cao LR. Methods for improving the power conversion efficiency of nuclear-voltaic batteries. Nucl Instrum Meth Phys Res A. 2019;927:133–139.
3. Xu J, Guo M, Lu M, He H, Yang G, Xu J. Effect of alpha-particle irradiation on InGaP/GaAs/Ge triple-junction solar cells. Materials. 2018;11:944.
4. Lu M, Wang R, Liu Y, Feng Z, Han Z, Hou C. Displacement damage dose approach to predict performance degradation of on-orbit GaInP/GaAs/Ge solar cells. Instrum Meth Phys Res B 2013;307:362–365.
5. Karim E, Demaree JD, Guardala N, Al-Sheikhly M. Elucidation of the mechanisms of protons and alpha particles-induced damages on the surface region of 4H SiC. 2nd International Conference on Ionizing Processes. ICIP; 2018.
6. Colerico CW, Serreze HB, Messenger SR, Burke EA, Xapsos MA. Alpha particle simulation of space radiation damage effects in semiconductor devices. IEEE Trans Nucl Sci. 1995;42(6).
7. Rybicki G, Vargas-Aburto C, Uribe RM. Silicon carbide alphavoltaic battery. 25th IEEE Photovoltaics Special Conference; 1996.
8. Sychov M, Kavetsky A, Yakubova G, Walter G, Yousaf S, Lin Q, Chan D, Socarras H, Bower K. Alpha indirect conversion radioisotope power source. Appl Radiat Isot. 2008;66:173–177.
9. Robbins DJ. Predicting the maximum efficiency of phosphor systems excited by ionizing radiation. J Electrochem Soc. 1980;127:2694.
10. Dai Y, Kum H, Slocum MA, Nelson GT, Hubbard SM. High efficiency single-junction InGaP photonvoltaic devices under low intensity light illumination. IEEE 44th Photovoltaic Specialist Conference; 2017.
11. Zein R, Alghoraibi I. Effect of deposition time on structural and optical properties of ZnS nanoparticles thin films. Int J Chem Technol Res. 2014;6(5):3220–3227.

12. Dimitrova V, Tate J. Synthesis and characterization of some ZnS-based thin film phosphors for electroluminescent device applications. Thin Solid Films. 2000;134:365.

13. Emy M, Tjipto S, Dessy P. Growth of ZnS:Ag:Cu thin films deposited on glass substrates using thermal evaporation technique for alpha-photovoltaic. Indonesian J Mater Sci. 2019;21(1):8–12.

14. Lee SS, Byun K-T, Park JP, Kim SK, Lee JC, Chang S-K, Kwak H-Y, Shim I-W. Homogeneous ZnS coating onto TiO_2 nanoparticles by a simple one pot sonochemical method. Chem Eng. 2008;139:194–197.

15. Li J, Zhang JZ. Optical properties and applications of hybrid semiconductor nanometarials. Coord Chem Rev. 2009;253(23–24):3015–3041.

16. Schneider S, Kocher DC, Kerr GD, Scofield PA, O'Donnell FR, Mattsen CR, Cotter SJ, Bogard JS, Bland JS, Wiblin C. Systematic radiological assessment of exemptions for source and byproduct materials. NUREG-1717; 2001.

17. Alig RC, Bloom SL. Electron-hole-pair creation energies in semiconductors. Phys Rev Lett. 1975;35(22):1522.

18. Hong L, Tang X-B, Xu Z-H, Liu Y-P, Chen D. Radioluminescent nuclear batteries with different phosphor layers. Nucl Instrum Meth Phys Res B. 2014;338:112–118.

19. Summers GP, Burke EA, Shapiro P, Messenger SR, Walters RJ. Damage correlations in semiconductors exposed to gamma, electron and proton radiations. IEEE Trans Nucl Sci. 1993;40:6.

20. Stan MA, Sharps PR, Fatemi NS, Spadafora F, Aiken D, Hou HQ. Production of extremely radiation hard 26% InGaP-GaAs-Ge triple junction solar cells. IEEE; 2000.

List of Symbols, Abbreviations, and Acronyms

αV	alphavoltaic
αPV	alpha-photovoltaic
Ag	silver
Al	aluminum
AlN	aluminum nitride
ARL	Army Research Laboratory
Cu	copper
DEVCOM	US Army Combat Capabilities Development Command
EHP	electron-hole pair
EPD	electrophoretic deposition
GaN	gallium nitride
IEL	ionizing energy loss
InGaP	indium gallium phosphide
IPA	isopropyl alcohol
I_{sc}	short circuit current
IV	current-voltage
LC	lattice constant
LET	linear energy transfer
MPP	maximum power point
NIEL	nonionizing energy loss
PV	photovoltaic
RF	radio frequency
SiC	silicon carbide
SRIM	Stopping and Range of Ions in Matter
UWBG	ultrawide bandgap
V_{oc}	open circuit voltage
WBG	wide bandgap
ZnS	zinc sulfide

1 (PDF) DEFENSE TECHNICAL INFORMATION CTR DTIC OCA

1 (PDF) DEVCOM ARL FCDD RLB CI TECH LIB

7 (PDF) DEVCOM ARL FCDD RLA M WRABACK FCDD RLA GA N BARBIERI FCDD RLA GC M RESTAINO V PARAMESHWARAN M LITZ FCDD RLA LE L LARKIN FCDD RLA MF J DEMAREE